

Photoemission and in Situ XRD Investigations on CuCoZnAl-Mixed Metal Oxide Catalysts for the Oxidative Steam Reforming of Methanol

S. Velu^{*,†} and Kenzi Suzuki

Ceramics Research Institute, National Institute of Advanced Industrial Science and Technology, Nagoya 463-8560, Japan

Chinnakonda S. Gopinath^{*,‡}

Catalysis Division, National Chemical Laboratory, Dr. Homi Bhabha Road, Pune 411 008, India

Received: April 18, 2002

A series of CuCoZnAl-multicomponent mixed oxide catalysts with various Cu/Co atomic ratios were prepared by the thermal decomposition of CuCoZnAl-hydrotalcite (HT)-like precursors at 450 °C in static air atmosphere. The XRD of calcined materials revealed the formation of a mixture of CuO and ZnO, Co₃O₄, and/or ZnCo₂O₄ depending on the chemical compositions. Core-level XPS and X-ray induced Auger electron spectroscopy (AES) revealed unambiguously the existence of Cu²⁺, Co²⁺, and Co³⁺ species in the calcined materials. Upon H₂-reduction at 300 °C, the Cu²⁺ was reduced to a mixture of Cu⁺ and Cu⁰, while Co³⁺ was reduced to Co²⁺. This was further supported by the in situ XRD of the reduced samples. Valence band (VB) photoemission studies demonstrated that the overlap between 3d bands of Cu and Co was marginal in calcined materials, however it was very high in the reduced samples. These mixed oxides were tested as catalysts in the oxidative steam reforming of methanol (OSRM) reaction for the production of H₂ in order to understand the effect of substitution of Co in the CuZnAl-oxide system. The Cu-rich catalyst, without Co, offered the highest H₂ production rate of about 200 mmol kg⁻¹ s⁻¹ with about 100% methanol conversion at 290 °C. Only trace amounts of CO were noticed. Introduction of Co decreased the H₂ production rate as the Co-containing species favored the hydrogenation of CO/CO₂ to CH₄ under the reaction operating conditions.

1. Introduction

Cu–Co based mixed oxides are known as promising catalysts for methanol and higher alcohol synthesis because of their attractive properties such as higher stability, higher activity at relatively low pressure, and higher selectivity toward alcohols rather than hydrocarbons.^{1–7} These catalysts are also active in the CO oxidation and CO hydrogenation (Fischer–Tropsch synthesis).⁸ The activity of these catalysts is strongly influenced by the method of preparation, thermal treatment, etc.^{3,4} It has been widely accepted that the catalysts derived from hydrotalcite (HT)-like hydroxycarbonate precursors synthesized by the coprecipitation of divalent (example, Cu, Co, Zn) and a trivalent (example Al) metal ion in the same crystalline structure provides, at relatively lower temperature (around 450 °C), well interdispersed mixed metal oxides with high surface area, and small and fairly uniform particle sizes and as a consequence a better catalytic activity, not only in the methanol and higher alcohol synthesis but also in the alkylation and hydroxylation of phenol, oxidation of cresols, etc.^{5,9–12}

Although the Cu–Co-based catalysts were developed several decades ago for the synthesis of alcohols, little is known about the chemical nature of Cu and Co and the interaction between them. It has been speculated that the existence of Cu–Co synergism is responsible for oxygenate formation.⁴ Character-

ization techniques such as X-ray diffraction (XRD), temperature-programmed reduction (TPR), X-ray photoelectron spectroscopy (XPS), IR, Mössbauer, etc., have been employed to understand the nature of interaction between Cu and Co in these mixed oxide catalysts and different conclusions have been made.^{3–7,12–15} A detailed literature survey indicates that no systematic XPS, X-ray induced Auger electron spectroscopy (AES), and in situ XRD studies have been reported to understand thoroughly the chemical nature of Cu and Co and the interaction between them.

It is generally accepted that the catalyst active for the synthesis of methanol is also active for the reforming of methanol to produce H₂ and carbon oxides, as the later reaction is the reverse of the methanol synthesis.^{16–18} Thus, the CuZnAl and CuZnAl(Zr)-mixed oxide catalysts derived from similar hydroxy carbonate precursors, known for the methanol synthesis, have been employed recently for the steam reforming and oxidative steam reforming of methanol (OSRM) reaction for the production of H₂ for fuel cell applications.^{18–24} Since the CuCo-based mixed oxide catalysts are also active in the CO oxidation and hydrogenation reactions, in addition to the methanol and higher alcohols synthesis, it has been intended to investigate the effect of the substitution of Co in the CuZnAl-mixed oxide catalysts in the OSRM reaction for H₂ production.

The objectives of the present study was therefore to investigate systematically the electronic nature of Cu and Co species and the interaction among them in the calcined (oxidized) and reduced samples by means of a combined XPS, AES, and in situ XRD techniques and then to understand the effect of Co substitution on the catalytic performance in the OSRM reaction.

* Author to whom correspondence should be addressed.

† Present Address: The Energy Institute, Department of Energy and Geo-Environmental Engineering, The Pennsylvania State University, 209 Academic Projects Building, University Park, PA 16802. E-mail: vxs23@psu.edu.

‡ Fax: 91-20-589 3761. E-mail: gopi@cata.ncl.res.in.

TABLE 1: Chemical Composition, Structural and Textural Properties of CuCoZnAl-Mixed Oxide Catalysts

catalyst	chemical composition (atomic ratio) ^a				XRD phase obtained		BET SA (m ² g ⁻¹)	pore volume (cc g ⁻¹) ^c
	Cu	Co	Zn	Al	uncalcined	calcined ^b		
CuCoC-1	2.53	0.00	0.77	1	HT + MT	CuO + ZnO	71	0.45
CuCoC-2	1.73	0.75	0.77	1	HT + MT	CuO + ZnO + Co spinel	94	0.61
CuCoC-3	1.35	1.17	0.83	1	HT + MT	CuO + Co spinel	84	0.43
CuCoC-4	0.88	1.59	0.81	1	HT	CuO + Co spinel	42	0.30
CuCoC-5	0.00	2.27	0.81	1	HT	Co spinel	40	0.29

^a Chemical composition of the catalyst precursors determined by X-ray fluorescence spectroscopy. ^b Samples calcined at 450 °C/5 h in static air atmosphere. ^c BET surface area and pore volume of the calcined samples determined by N₂ adsorption–desorption method. HT = Hydrotalcite (JCPDS file No. 37-629). MT = Malachite [Cu₂(OH)₂CO₃] (JCPDS file No. 41-1390).

2. Experimental Section

2.1. Synthesis of CuCoZnAl-Mixed Oxide Catalysts and Characterization. CuCoZnAl-HTs with different Cu:Co ratios were synthesized by a coprecipitation method at 298 K by reacting aqueous solutions containing a mixture of M^{II}(NO₃)₂ (M^{II} = Cu, Co, Zn) and Al(NO₃)₃ as precursors and a mixture of NaOH (≈2 M) and Na₂CO₃ (≈0.3 M) as precipitants at a constant pH (≈9) as described earlier.²⁵ The as-synthesized samples were calcined at 450 °C for 5 h in a muffle furnace at a heating rate of 10 °C/min to obtain CuCoZnAl-mixed oxide catalysts. Experimental details for chemical analysis using X-ray fluorescence spectroscopy (XRF), XRD, TPR, and BET surface area measurements are provided in the earlier publications.^{20,25}

X-ray photoelectron spectra (XPS) were acquired on a VG Microtech Multilab ESCA 3000 spectrometer equipped with a twin anode of Al and Mg. All measurements were made at room temperature using a nonmonochromatized Mg Kα X-ray source (hν = 1253.6 eV) on powder samples. Base pressure in the analysis chamber was maintained at 10⁻¹⁰ Torr range. The energy resolution of the spectrometer was set at 0.8 eV with Mg Kα radiation. Binding energy (BE) was calibrated with respect to Au 4f_{7/2} core level at 83.9 eV. The BE of adventitious carbon (284.9 eV) was utilized for charge correction. The error in all the BE values reported is ±0.1 eV.

In situ XRD patterns of all the calcined samples were obtained on a Rigaku X-ray diffractometer (Rint 2000 model) in the 2θ range 5–70° at a scan rate of 2°/min. The powder sample was pressed on a Pt sample holder fitted within a special cell. The instrument was programmed in such way that the XRD pattern of the sample was measured initially at 30 °C and at ambient atmosphere. The sample was then heated to 300 °C at a heating rate of 5 °C/min in 5% H₂/Ar flow (50 cm³/min) through the special cell and maintaining this temperature for 3 h before the XRD pattern was recorded. The sample was then cooled (5 °C/min) to 200 °C either in H₂/Ar gas mixture or in N₂ atmosphere and the XRD pattern at this temperature was also recorded.

2.2. Catalytic Activity Measurements. The OSRM reaction was performed in a conventional fixed-bed flow reactor (4 mm i.d.) using 100 mg of the catalyst (grain size 0.30–0.355 mm) in the temperature range 180 to 290 °C at atmospheric pressure. The catalyst was reduced in a H₂ stream (10–20 cm³/min) from room temperature to 300 °C at a heating rate of 5 °C/min and maintaining this temperature for 3 h before cooling down to the reaction temperature. Subsequently, premixed water and methanol with a H₂O/CH₃OH molar ratio = 1.6 was fed into the preheater by means of a micro-feeder (flow rate = 2.0 cm³/h). Synthetic air (20.2 vol % of O₂ in N₂) was fed at a rate of 10 to 20 cm³/min (O₂/CH₃OH molar ratio = 0.25). A detailed experimental procedure on the activity measurement and the method of product analysis is described elsewhere.^{19–21}

3. Results

3.1. Characterization of Calcined Samples. *3.1.1. Bulk Characterization (chemical analysis, XRD, and TPR).* The chemical compositions, structural and textural properties of CuCoZnAl-mixed oxide catalysts prepared in the present study are given in Table 1. Detailed structural, textural, and redox properties of uncalcined as well as calcined CuCoZnAl-HT-like materials using XRD, TG/DTA, UV–visible diffuse reflectance spectroscopy and TPR have been reported recently,²⁵ and hence they are described here briefly. The XRD patterns of the as-synthesized materials corresponded to those typical of the layered rhombohedral structure of HT-like layered double hydroxides (LDHs; JCPDS file No. 37-629). Upon calcination, the Cu-rich sample (CuCoC-1) exhibited a diffraction pattern attributed to a mixture of CuO and ZnO phases (Table 1). Substitution of Co for Cu decreased the crystallinity of CuO and ZnO phases with a concomitant increase in the crystallinity of a cobalt-based spinel similar to that of Co₃O₄. The Co-rich CuCoC-5 exhibited a relatively well-crystallized Co-spinel. No ZnO phase was detected in the Co-containing catalysts. The catalysts derived from intermediate compositions contained a mixture of CuO and Co-based spinel phases.

The TPR profiles of all samples calcined at 450 °C are shown in Figure 1. The specimens CuCoC-1 through CuCoC-4 containing Cu exhibit a sharp H₂ consumption peak around 200 °C. A comparison of the TPR results with those of pure CuO and similar Cu-based mixed oxide systems revealed that H₂ consumption in this region corresponds to reduction of the CuO phase. On the other hand, the Co-rich CuCoC-5, without copper, exhibits strong H₂ consumption bands at ca. 360 and 680 °C, indicating the existence of two kinds of reducible Co species. Note that, under our experimental conditions, the pure samples of CoO (Co²⁺) as well as Co₃O₄ (Co^{3+/2+}) have been reduced in the same reduction region around 360 °C.²⁶ In contrast, the pure CoAl₂O₄ (Co²⁺ with Al³⁺ neighbors) were reduced at ca. 700 °C. Since, the XRD indicated the presence of a Co-based spinel rather than CoO phase, the H₂ consumption in the first reduction region can be assigned to the reduction of Co₃O₄-like species or ZnCo₂O₄ spinel. On the other hand, the peak in the second reduction region can be ascribed to the reduction of Co-based spinel with Al³⁺ neighbors or Al-containing ZnCo₂O₄ solid solution. H₂ consumption due to these two kinds of Co species appears as weak bands around 380 and 600 °C in CuCoC-2, and the intensity of these bands increases with further increase in Co content. It is interesting to note that the position of the peak corresponding to the reduction of CuO gradually shifts to lower temperatures with increasing Co content, from 230 °C for CuCoC-1 to 170 °C for CuCoC-4. Though, the shift in the peak position corresponding to the reduction of Co species is not clearly discernible due to their weak H₂ consumption bands, a careful analysis of TPR profiles indicates a shift of

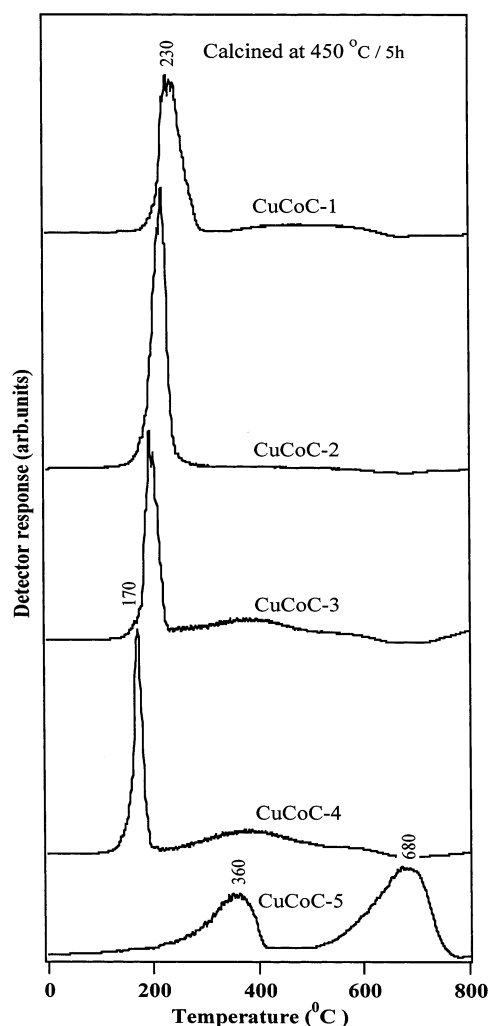


Figure 1. TPR profiles of CuCoZnAl-mixed oxide catalysts. Note the gradual shift in the peak position around 200 °C toward lower temperature with increasing Co content.

about 20 °C on moving from CuCoC-3 to CuCoC-5. In other words, the peak corresponding to the reduction of Co species (in the first reduction region) shifts toward higher temperature with increasing Cu content (from 360 °C for CuCoC-5 to ca. 380 °C for CuCoC-2). These results suggest that the substitution of Co^{2+} in the CuZnAl-HT improve the reducibility of CuO. In contrast, substitution of Cu for Co in the CoZnAl-HT framework impedes the reducibility of Co species of the resulting mixed oxides.

3.1.2. Surface (XPS) Characterization. To distinguish the three oxidation states of Cu (Cu^0 , Cu^{1+} , Cu^{2+}), both the core emitted photoelectrons and the X-ray induced Auger electron spectroscopy (XAES) measurements could be undertaken. The Cu^{2+} species can be distinguished from Cu^{1+} and Cu^0 from the difference in the BE (>1 eV) and from the appearance of satellites. Since both Cu^{1+} and Cu^0 will have the same BE in the core level spectra, the XAES should be used to distinguish them. The modified Auger parameter (α') has been generally used to further confirm the chemical state of copper. The parameter α' is defined as²⁷

$$\alpha' = h\nu + (\text{KE Cu}_{\text{LMM}} - \text{KE Cu } 2p_{3/2}) \quad (1)$$

where, $h\nu$ is the energy of the incident photon, and $\text{KE Cu}_{\text{LMM}}$ and $\text{KE Cu } 2p_{3/2}$ are kinetic energies of Auger electron and $2p_{3/2}$ core level photoelectron, respectively.

TABLE 2: XPS and AES Parameters of CuCoZnAl-oxide Catalysts and Some Reference Compounds

compound	BE of Cu $2p_{3/2}$ (eV)	KE of Cu LMM (eV)	α' (eV)	ref
Cu	932.6	918.4	1851.0	29, 30
Cu_2O	932.4	916.5	1848.9	29, 30
CuO	933.8	917.6	1851.4	28
Malachite	934.6	916.8	1851.4	31
CuZnAl-HT	934.6	916.0	1850.6	31
CuAl_2O_4	935.0	916.5	1851.5	30
CuCoC-1	932.4	919.2	1851.6	present work
CuCoC-2	933.8	917.9	1851.7	present work
CuCoC-4	934.5	917.4	1851.9	present work
CuCoC-1R ^a	932.6	918.1, 916.5	1850.7, 1849.1	present work
CuCoC-2R ^a	932.6	918.1, 916.5	1850.7, 1849.1	present work
CuCoC-4R ^a	932.6	918.1, 916.5	1850.7, 1849.1	present work

^a Data from reduced catalysts.

Figure 2 displays the Cu 2p core level XPS (left panel) and the XAES (right panel) for a few representative samples, namely, CuCoC-1 (contains Cu with no Co), CuCoC-2 (contains both Cu and Co with $\text{Cu/Co} \approx 2$), and CuCoC-4 ($\text{Cu/Co} \approx 0.5$). It can be noticed (see the left panel) that the catalyst CuCoC-1 exhibits the Cu $2p_{3/2}$ main peak at ca. 932.4 eV. The position of the peak shifts gradually toward higher BE with increasing Co content. This directly indicates that the electron density on Cu species is depleted with increasing Co concentration. In all cases, a strong satellite peak is observed on the higher BE side above 940 eV, indicating the existence of Cu^{2+} species. The intensity ratio between satellite and the main line (I_s/I_m) is > 0.50 , and close to that of pure CuO.²⁸ The full width at half-maximum (fwhm) of the main peak marginally decreases from ca. 3.6 eV for CuCoC-1 to ca. 3.3 eV for CuCoC-4, whereas the fwhm of the satellite peak increases from ca. 5.1 eV for CuCoC-1 to ca. 5.5 eV for CuCoC-4.

The Cu $\text{L}_{3\text{M}_{45}\text{M}_{45}}$ Auger spectra of samples are shown in Figure 2 (right panel). CuCoC-5 catalyst shows some peaks entirely due to Zn—Auger spectral features at 926.0 and 900–912 eV due to $\text{L}_{2\text{MM}}$ and $\text{L}_{3\text{MM}}$ transitions, respectively. In fact, the Zn-Auger features are much less in intensity ($<20\%$) compared to any of Cu-Auger features and really do not contribute significantly to any of the changes that are observed in the Cu-Auger spectrum. It can be seen that the CuCoC-1 catalyst exhibits the Cu $\text{L}_{3\text{M}_{45}\text{M}_{45}}$ line at a kinetic energy (KE) of 919.2 eV. Note that for pure CuO this line appears at 917.6 eV. However, depending on the chemical environment and geometry, the position of this line has been found to shift significantly. The α' determined are given in Table 2 with the data of some of the reference samples reported in the literature.^{28–31} α' in the range 1851.6 to 1851.9 eV, which is close to that of CuO (1851.4 eV), has been obtained for CuCoC-1 to CuCoC-4 samples. A careful analysis reveals that there is a gradual decrease in energy and intensity of all the Auger peaks with increasing Co concentration, and this can be attributed to the distortion of Cu^{2+} environment. Such a distortion also improves the intensity of satellite peaks ca. 924 and 912 eV due to the activation of the $3d^8\text{L}$ to $3d^9\text{L}^2$ state and the $3d^{10}\text{L}$ ground state to the $3d^8\text{L}$ state transitions, respectively, where L indicates a hole on the ligand.³²

The Co 2p core level XPS and Co XAES of CuCoC-2, CuCoC-4, and CuCoC-5 are displayed in Figure 3. The results are compared with the XPS data of some of the Co-based oxides reported in the literature (Table 3).^{33,34} CuCoC-5 exhibits a Co $2p_{3/2}$ peak at 780.5 eV and a peak due to Co $2p_{1/2}$ at 795.6 eV, and satellites are weak in intensity and appear at 790.2 and 802.7 eV, respectively. The intensity of a satellite peak, particularly that of Co $2p_{1/2}$, decreases gradually with increasing Co content.

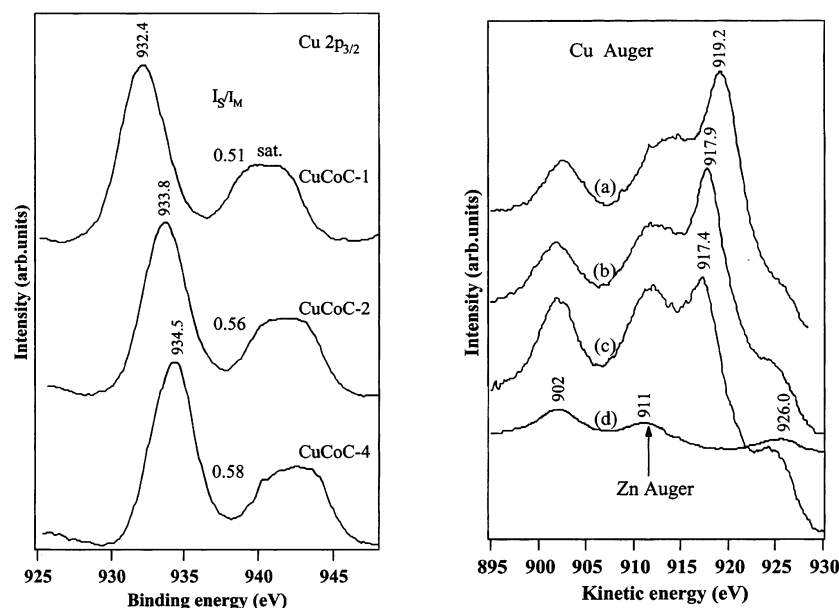


Figure 2. Cu 2p core level X-ray photoelectron spectra (left panel) and X-ray induced Cu LMM Auger electron spectra (right panel) of CuCoZnAl-mixed oxide catalysts. In both cases, the peak position shifts gradually with increasing Co content.

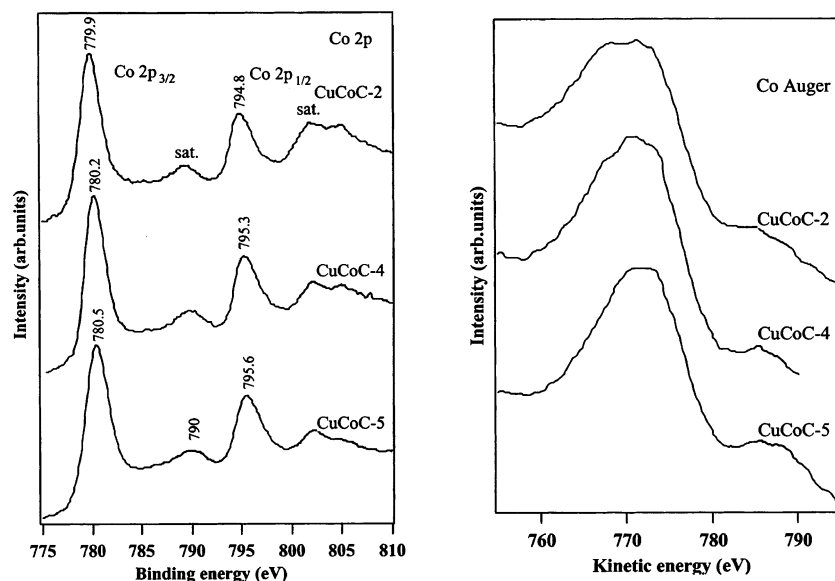


Figure 3. Co 2p core level X-ray photoelectron spectra (left panel) and X-ray induced Co LMM Auger electron spectra (right panel) of CuCoZnAl-mixed oxide catalysts. Note the decreasing bandwidth with increasing Co content.

Also to be noted are that the BE of the Co 2p_{3/2} level decreases with increasing Cu content while the energy separation between the spin-orbit doublets of the Co 2p levels remain at ca. 15 eV. However, the BE shift is rather small (about 0.8 eV) compared to that observed in the Cu 2p XPS (2 eV) level upon increasing Co content. The above observations are attributed to a change in the cation distribution in the spinel surface and/or an increase in the Co³⁺ concentration at the expense of Co²⁺ ions into the spinel lattice with increasing Cu content.

The Co L₃M₄₅M₄₅ spectra (Figure 3 right panel) of the same samples exhibit a broad and intense feature corresponding to the Auger transitions between 760 and 780 eV and a weak feature due to the L₂M₄₅M₄₅ transition between 780 and 790 eV. There is a clear and gradual narrowing of the main feature with increasing Co content. This result implies that more than one final state is contributing in CuCoC-2 and CuCoC-4 containing copper while only one final state is predominantly contributing in the CuCoC-5 without copper.

TABLE 3: Co 2p XPS Data from CuCoZnAl-oxide Catalysts and Some Co-containing Reference Materials^{33,34}

material	BE of Co 2p _{3/2} (eV)	reliability (eV)	shake-up satellite	energy gap between spin-orbit doublet (eV)
Co metal	778.7	±0.1		15.1
CoO	780.1	±0.9	strong	15.5
Co(OH) ₂	780.9	±0.2	strong	16.0
Co(NO ₃) ₂	781.9		strong	16.0
CoAl ₂ O ₄	781.7	±0.5	strong	15.5
Co ₃ O ₄	780.5	±0.7	weak	15.0
ZnCo ₂ O ₄	780.3		weak	15.0
Co ₂ O ₃	780.2	±0.7	weak	
CuCoC-2 ^a	779.9	±0.1	weak	14.9
CuCoC-4 ^a	780.2	±0.1	weak	15.1
CuCoC-5 ^a	780.5	±0.1	weak	15.1
CuCoC-2R ^a	780.9	±0.1	strong	15.9
CuCoC-4R ^a	780.8	±0.1	strong	15.9

^a Data collected in the present study. R indicates the data from reduced catalysts.

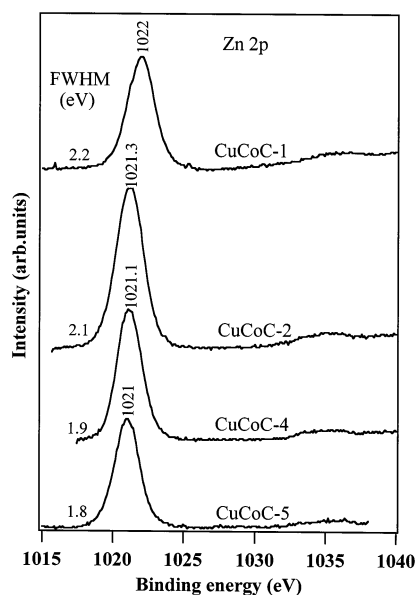


Figure 4. Zn $2p_{3/2}$ core level X-ray photoelectron spectra of CuCoZnAl-mixed oxide catalysts. A sudden drop in BE upon introduction of Co in the system (CuCoC-2) can be noticed.

The XPS of Zn $2p_{3/2}$ core level are presented in Figure 4. The CuCoC-1 exhibits a peak centering at 1022 eV, which is very close to the BE of ZnO (1021.6–1022 eV) reported in the literature.^{28,31} Substitution of Co for Cu results in an abrupt shift toward lower BE, and the BE of CuCoC-5 is 1021 eV. Further, a decrease in the fwhm of $2p_{3/2}$ peak from 2.2 eV for CuCoC-1 to 1.8 eV for CuCoC-5 can be noticed. The shift in BE and the narrowing of the Zn $2p_{3/2}$ peak upon increasing Co content observed clearly indicates that zinc plays a role in the electronic structure of these catalysts and is not a silent spectator. Porta and co-workers³⁵ have also observed a shift of about 0.8 eV in the Zn $2p_{3/2}$ BE with respect to a change in the Cu:Zn:Al ratio of the CuZnAl oxide catalysts prepared from hydroxycarbonate precursors. On the other hand, some researchers^{28,36} assumed that there was no chemical shift of Zn $2p_{3/2}$ in the similar CuZn-based mixed oxides and used its BE as an internal reference.

The valence band (VB) spectra can be expected to show a very significant difference with respect to the chemical composition since VB is associated with energy levels directly involved in chemical bonding. VB spectra obtained from XPS of CuCoC-1 to CuCoC-5 samples are presented in Figure 5. The main VB observed below 5 eV could have contributions from 3d orbitals of the Cu and Co and O 2p level. However, at the incident X-ray energy (1253.6 eV) employed in these experiments, the photoionization cross section (σ) value (O 2p = 0.0005, Zn 3d and Cu 3d = 0.021, and Co 3d = 0.0067 Mb)³⁷ is the dominating factor in formulating the spectral intensity. These data clearly suggest that the Cu 3d will have larger contributions to the VB and the contribution from O 2p is less significant. The VB assignments are straightforward for Cu-free and Co-free samples as they have only one peak at ca. 1.5 and 4.2 eV and the same is attributed to Co and Cu 3d orbitals, respectively. Cu- and Co-containing samples show two distinct features due to contribution from Cu and Co 3d orbitals. The Cu 3d band at 4.2 eV is very broad for CuCoC-1 compared to the Co 3d band at 1.5 eV for CuCoC-5. The position of the Cu 3d band shifts significantly on introduction of Co, but the reverse is not fully true. The Cu 3d band in CuCoC-2 occurs at 3.7 eV, and the Co 3d band appears at 1.1 eV. Further increase in Co content (CuCoC-4) moves the Co 3d band to 1.5 eV and Cu 3d band to 4.5 eV. However, introduction of Cu in the pure

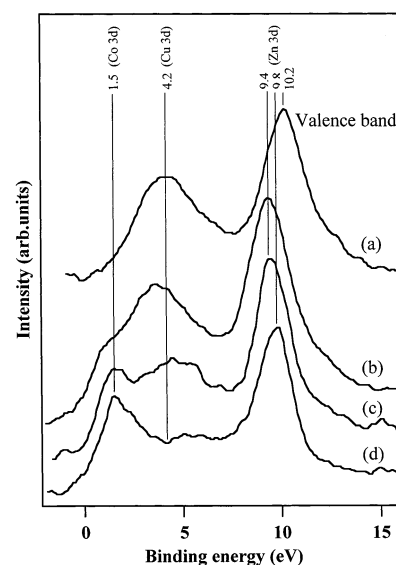


Figure 5. Valence band X-ray photoelectron spectra of CuCoZnAl-mixed oxide catalysts. (a) CuCoC-1, (b) CuCoC-2, (c) CuCoC-4, (d) CuCoC-5.

Co system does not change the energy of Co 3d orbitals. This indicates that the Cu 3d orbitals are relatively easily perturbed by the presence of Co.

Based on σ and expected energy of completely filled Zn 3d ($3d^{10}$) orbitals, the peak at 10 eV can be attributed to Zn 3d orbitals. It can be seen from Figure 5 that there is a clear shift in the Zn 3d orbitals around 10 eV with respect to the Cu/Co atomic ratio. For instance, the peak maximum is centered at 10.2 eV in the case of CuCoC-1. Introduction of Co results in a sudden decrease in the BE of Zn 3d to 9.3 eV in CuCoC-2, very much like the Zn 2p core level. However, the position gradually shifts again to high BE and narrowed down with further increasing Co content. The Co-rich CuCoC-5 shows the Zn 3d band maximum at 9.8 eV, which is about 0.4 eV less than that of the CuCoC-1. The observed shift in the Zn 3d level with respect to the Cu/Co ratio in these materials further substantiates the results observed in the Zn 2p core level (Figure 4) and the involvement of Zn 3d orbitals in the electronic structure of the catalysts. Additionally, the energy gap between Zn 3d and Cu 3d orbitals decreases from 6.2 eV for CuCoC-1 to 5 eV for CuCoC-4. Contrarily, the energy gap between Zn and Co 3d orbitals remains close to 8.2 eV. This clearly suggests that there exists a strong interaction between Zn and Cu and the interaction between Zn and Co is very weak or none. Although the energy gap between Zn 3d and Cu 3d orbitals is more than 5 eV to have a direct interaction, the above changes in energy gap suggests that the interactions are indirect. It is likely that the CuO particles are covered by ZnO in these materials, as confirmed from the surface quantitative estimation. It is also noted that, in the Co-containing samples, the topmost band consists of mainly Co 3d orbitals and hence it is expected that the physicochemical and redox properties of these catalysts are dominated by the Co-based phases. This is in agreement with the TPR results, which indicated that the reducibility of copper species is augmented with increasing Co content in the sample (see Figure 1).

3.2. Characterization of Reduced Samples. 3.2.1. Bulk (in situ XRD) Characterization. XRD patterns of all the calcined samples were recorded under ambient conditions followed by in situ reduction at 300 and 200 °C using 5% H_2 in Ar. Figure 6 depicts the in situ XRD patterns of four samples. In situ reduction of CuCoC-1 at 300 °C is so effective that only Cu-

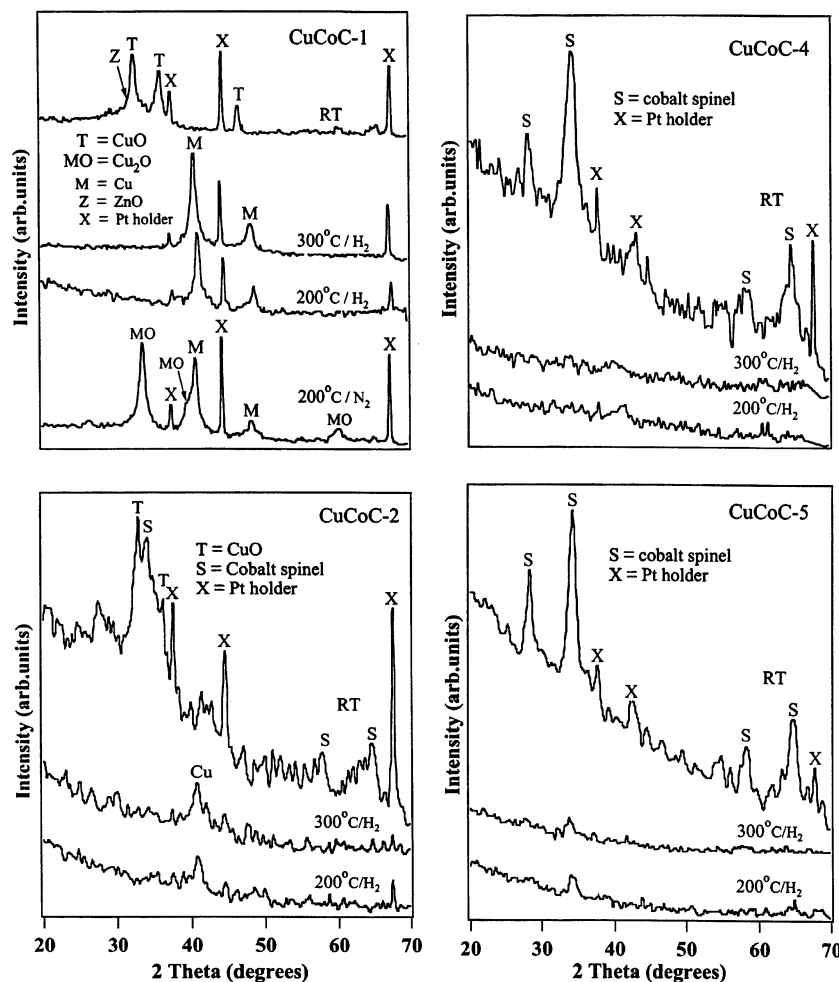


Figure 6. In situ XRD patterns of CuCoZnAl-mixed oxide catalysts. Metallic Cu peaks are observed predominantly in all cases in H_2 atmosphere and a mixture of metallic Cu and Cu^{+} in N_2 atmosphere.

metal is seen and peaks due to CuO just disappear. Cu remains in the metallic state even at 200 °C in the H_2/Ar atmosphere. Nonetheless, the formation of a Cu_2O phase is observed with metallic Cu when N_2 gas replaces the H_2/Ar gas in the later step. In the cases of CuCoC-2 and CuCoC-4, containing CuO and Co_3O_4 -like spinel phases before reduction, only metallic Cu is seen in the in situ XRD at 300 °C. Peaks due to the Co_3O_4 -like spinel were completely destroyed and no other phase can be detected. However, in CuCoC-5, after reduction at 300 °C, a Co_3O_4 -like spinel is detected with low intensity, implying a partial destruction of the spinel phase. The above results indicate that the CuO phase undergoes complete reduction to metallic Cu while the Co-spinel is partially reduced. Apparently, the reduced samples appear amorphous-like and it is difficult to ascertain the nature of Co-based phases produced upon reduction.

3.2.2. Surface (XPS) Characterization. To investigate the nature of Cu and Co species on the surface of the reduced catalysts, they were subjected to XPS characterization after reduction in H_2 atmosphere at 300 °C for 3 h. Reduction was performed ex situ in a vertical down-flow reactor, similar to that used for the catalytic experiments, and then cooled to room temperature. The reduced samples were removed from the reactor carefully under dry nitrogen atmosphere and transferred to the XPS chamber within a few minutes.

XPS data of the Cu and Co core levels are included in Tables 2 and 3. The Cu Auger, Al 2p and 3p core level spectra of metal ions, and VB spectra of the reduced samples are shown

in Figures 7, 8, and 9, respectively, and are compared with those of the calcined samples. These three sets of spectra reflect all the changes observed upon reduction treatment. The Cu 2p core level XPS showed a clear single peak at 932.6 eV without any satellite at a higher BE. The Cu $L_{3M_{45}M_{45}}$ Auger spectra from reduced samples together, with that of the CuCoC-4 calcined sample and the Zn–Auger spectrum of CuCoC-5, are shown in Figure 7. It is very clear that the reduced samples exhibit a double peak structure at KE values of 916.5 and 918.1 eV. It is to be noted that the unreduced samples exhibit a single peak at 917.4 eV in this region (Figure 2). The relative intensity of the low energy peak at 916.5 eV increases compared to the peak at 918.1 eV with decreasing Cu content in the sample. The α' values of the low and high KE peaks have been calculated to be 1849.1 and 1850.7 eV, respectively. These values are in good agreement with those reported for Cu_2O and metallic Cu, respectively (Table 2). However, no peak due to CuO has been detected either in the Cu 2p or in the XAES of the reduced samples, indicating that all of the Cu^{2+} species in these catalysts are reduced to Cu^{1+} and Cu^0 and in excellent agreement with the in situ XRD results.

To extract quantitative information regarding Cu^0 and Cu^{+} , an attempt has been made to calculate the Cu^0/Cu^{+} ratio on the surface of these reduced samples from the XAES by differential analysis. Owing to a very significant overlap of the Auger transitions of Cu^0 and Cu^{+} and a large background in the spectra, the determination of the Cu^0/Cu^{+} ratio is somewhat tedious. In this study, the Shirley background of the original spectra was

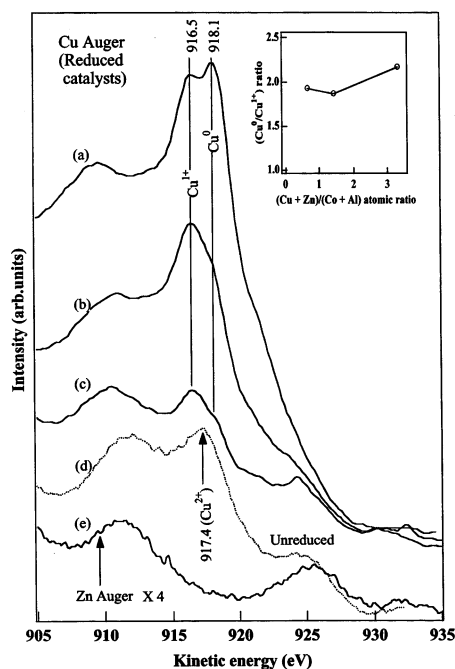


Figure 7. X-ray induced Cu LMM Auger electron spectra of CuCoZnAl-mixed oxide catalysts reduced at 300 °C; (a) CuCoC-1, (b) CuCoC-2, (c) CuCoC-4, (d) CuCoC-4 calcined, (e) Zn-Auger spectrum of CuCoC-5. Inset shows the variation of the $(\text{Cu}^0/\text{Cu}^{1+})$ ratio with respect to the $(\text{Cu} + \text{Zn})/(\text{Co} + \text{Al})$ atomic ratio.

corrected first and then differential spectra were plotted. The inset in Figure 7 shows the dependence of the Cu^0/Cu^+ ratio as a function of the $(\text{Cu} + \text{Zn})/(\text{Co} + \text{Al})$ atomic ratio. It can be seen that the Cu^0/Cu^+ ratio is the highest for the Cu-rich CuCoC-1 catalyst and the ratio decreases with increasing Co content. This indicates that the Cu^+ is being stabilized on the surface of the catalyst with increasing Co content.

The Co 2p XPS data of some of the reduced samples are included in Table 3. The Co $2p_{3/2}$ and $2p_{1/2}$ peaks appeared at higher BEs with a larger energy gap (15.9 eV) between the spin-orbit doublets compared to the 15 eV value observed on calcined samples. These parameters are very close to those observed for Co^{2+} species in $\text{Co}(\text{OH})_2$ (Table 3). Besides, the satellite intensity increased remarkably. Further, the Co 2p XPS did not exhibit any feature due to Co metal. These results infer that, upon reduction at 300 °C, the Co^{3+} species are reduced to Co^{2+} species.

Figure 8 displays the photoemission from Al 2p and 3p core levels of transition metal ions. 3p core level spectra from Cu and Co are in excellent agreement with their respective 2p core level counterpart and essentially the same information is obtained. The Co 3p core level, like Co 2p, shows a strong satellite after reduction, which is not seen on calcined catalysts. This unambiguously explains the reduction of Co^{3+} to Co^{2+} due to hydrogen treatment. A relatively larger intensity of the Co 3p level from reduced catalysts also hints the segregation of Co to the surface. In a similar manner, copper reduction from Cu^{2+} on calcined catalysts to metallic Cu and Cu^+ is evident from Cu 3p spectra after reduction. The Al 2p level is seen clearly on calcined catalysts despite some overlap with Cu 3p. Further, there is a huge overlap between Al 2p and Cu 3p after hydrogen treatment, since the energy of Cu 3p levels moves to a lower BE as a result of reduction of copper. The Al 2p core level appears at the same BE of 73.8 ± 0.2 eV, for all catalyst compositions before and after reduction. This hints that the electron density on Al remains the same, irrespective of different

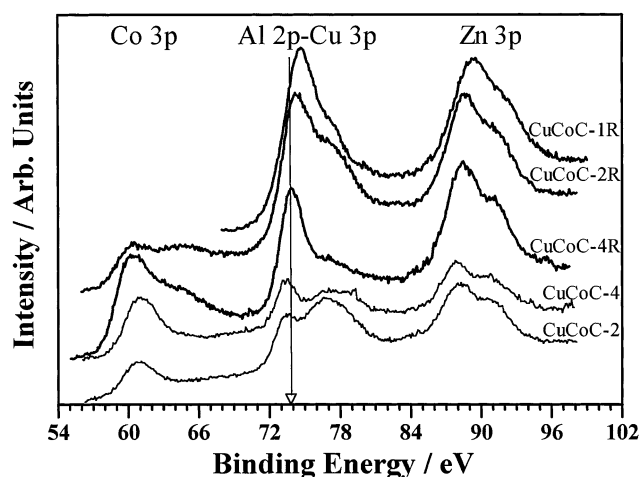


Figure 8. Al 2p and metal ions 3p XPS for calcined and reduced catalysts. The same BE observed for Al 2p core level indicates the electron density remains the same after reduction too.

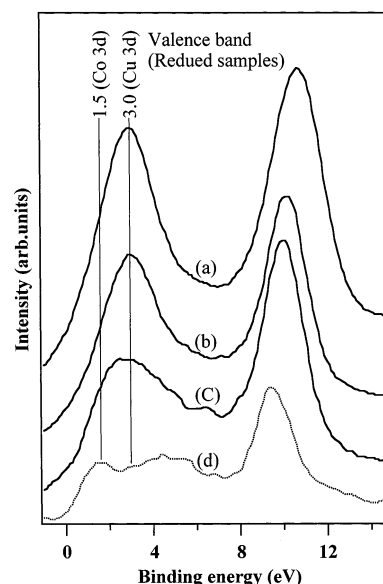


Figure 9. Valence band XPS of CuCoZnAl catalysts ((a) CuCoC-1R, (b) CuCoC-2R, (c) CuCoC-4R, and (d) CuCoC-5R) reduced at 300 °C; note the strong overlap between the Cu 3d and Co 3d bands in these materials and a total overlap of the Co 3d bands in CuCoC-2. The intensity at Fermi level ($E_F = 0$) increases with increasing copper content.

compositions and reduction conditions employed. The Zn 3p core level shows a decrease in BE with increasing Co content after reduction, in line with Zn 2p core level results from calcined and reduced catalysts.

The VB spectra are recorded for all reduced samples and the results are shown along with that of calcined samples in Figure 9. A comparison of the VB spectra of reduced and calcined samples reveals the following very interesting changes. (a) The BE of Cu 3d energy level decreases from about 4 eV for calcined samples (see also Figures 6–8) to about 3 eV for all reduced samples. (b) The BE of the Co 3d energy level instead increases from 1.5 eV for calcined samples to about 2.5 eV in reduced samples. (c) The BE of the Zn 3d level increases by about 0.6 eV compared to its calcined counterparts. However, the Zn 3d levels move closer to the main VB as Co content increases. (d) The energy gap between Zn 3d and Cu 3d levels increases to ≥ 7.2 eV for reduced samples compared to ≤ 6.2 eV for calcined samples. (e) The energy gap between Zn and Co 3d levels remains around 8 eV. (f) The peak intensity is very significant

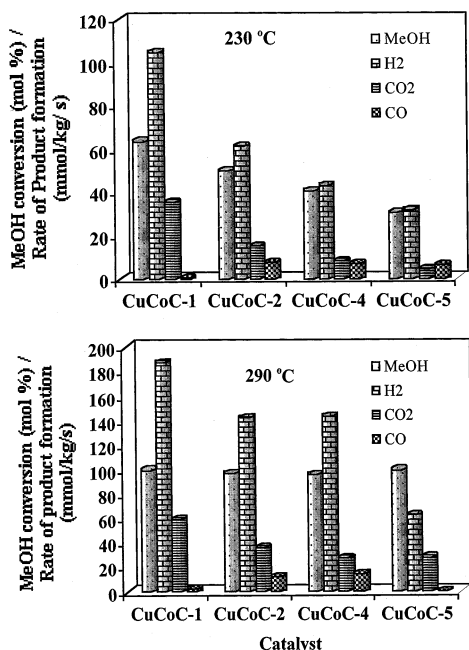
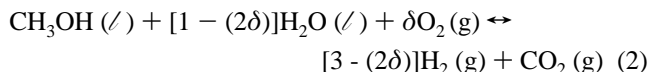


Figure 10. Catalytic performance of CuCoZnAl-mixed oxides in the oxidative steam reforming of methanol for H₂ production. Data collected at the reaction temperatures 230 °C (top panel) and 290 °C (bottom panel) are shown.

at the Fermi level ($E_F = 0$ eV) on reduction compared to very poor or no intensity at E_F from calcined samples and on the whole the main VB moves toward E_F as the Co content increases.

3.3. Catalytic Oxidative Steam Reforming of Methanol.

The catalytic performance of CuCoZnAl-mixed oxides was tested in the OSRM reaction for H₂ production (eq 2):



For $\delta = 0.25$, $\Delta H^\circ_{298} = -12.0$ kJ mol⁻¹ and $\Delta G^\circ_{298} = -109.6$ kJ mol⁻¹. Prior to the reaction, the Cu-containing catalysts were reduced in pure H₂ at 300 °C for 3 h while the Cu-free CuCoC-5 was reduced at 700 °C for 3 h. The OSRM reaction was performed at 230 and 290 °C and the results are compared in Figure 10. At 230 °C, the Cu-rich CuCoC-1 exhibits about 60% methanol conversion with a H₂ production rate of about 100 mmol kg(catalyst)⁻¹ s⁻¹. Substitution of Cu by Co, however, decreases both methanol conversion and the rate of H₂ production while the rate of CO production increases. The CuCoC-5 without Cu exhibits the lowest methanol conversion of about 30% with a CO production rate of about 6 mmol kg⁻¹ s⁻¹. In contrast, the catalytic activity for methanol conversion increases close to 100% and it remains unchanged for all compositions at a reaction temperature of 290 °C. Under this condition, the rate of H₂ production over the CuCoC-1 catalyst is the highest, about 190 mmol kg⁻¹ s⁻¹ while it is about 150 mmol kg(catalyst)⁻¹ s⁻¹ over both CuCoC-2 and CuCoC-4. The rate of CO₂ production also decreases with a consequent increase in the rate of CO production over these later catalysts. Interestingly, the rate of CO production decreases dramatically to about 0.5 mmol kg⁻¹ s⁻¹ over the CuCoC-5 catalyst. Although this catalyst offers the lowest CO outlet level, the H₂ production rate is low (65 mmol kg⁻¹ s⁻¹) in comparison with that obtained over the CuCoC-1 catalyst. These results indicate that substitution of Co for Cu in the CuZnAl-mixed oxide

catalyst system favors the hydrogenation of CO to CH₄ rather than CO oxidation to CO₂ in the secondary reaction.

4. Discussion

4.1. Chemical States of Cu and Co in the Calcined Catalysts. The satellites in Cu and Co 2p XPS (Figures 2 and 3) are due to interaction between core hole and valence electrons, which results in a change of potential seen by the valence electrons upon creation of the core hole. The appearance of satellites is also an indication of the existence of Cu²⁺ and Co^{2+/3+} species. For compounds containing Cu²⁺, the main peak and satellite correspond to a final state of 2p⁵3d¹⁰L and 2p⁵3d⁹, respectively.³² The satellite structure is a result of multiplet splitting in the 2p⁵3d⁹ state. Similarly, the main and satellite peaks of Co²⁺ are attributed to 2p⁵3d⁸L and 2p⁵3d⁷ final states,⁸ respectively. Note that for octahedrally coordinated diamagnetic Co³⁺ (3d⁶, i.e., t_{2g}⁶ e_g⁰), the satellite peak would be virtually absent or very weak due to changes in energy of different final states. Among the Co³⁺ 2p core level photoemission final states, the 2p⁵3d⁷L configuration screens the 2p core hole more effectively than the 2p⁵3d⁶ configuration and hence there is an energy reversal in the final states.³⁸ This creates a large energy gap between the main and satellite lines in the Co³⁺ system and hence a poor intensity satellite or no satellite in such systems.

In Cu XPS, the I_s/I_m ratio between 0.5 and 0.6 and the α' in the range 1851.6 to 1851.9 eV (Figure 2 and Table 2), which are very close to that of CuO, suggest that CuO-like species are present in these catalysts. On the other hand, the very low I_s/I_m ratio of about 0.1 observed in Co 2p XPS strongly suggests that cobalt is present in both Co²⁺ and Co³⁺ oxidation states. The observed energy separation of ca. 15 eV between spin-orbit doublets of Co 2p levels together with the appearance of weak satellites reveals the formation of Co₃O₄ and/or ZnCo₂O₄ spinel, wherein a major part of Co exists in the 3+ oxidation state.^{8,33–34} The broad feature seen in Co Auger spectra of these samples also supports the existence of Co²⁺ and Co³⁺ species. The Co 2p XPS peaks attributed to Co²⁺ and Co³⁺ are, however, unresolved as their BEs are very close to each other. For instance, the BE of Co²⁺ and Co³⁺ in Co₃O₄ are 780.7 and 779.6 eV, respectively.³³ Note that the BE of Co³⁺ is lower than that of Co²⁺ in these compounds owing to a large increase in the covalency of Co³⁺–O bonding compared to that of Co²⁺–O bonding in the crystal lattice. Jimenez et al.³⁹ attributed this “inverse shift” to the semiconductor properties of Co₃O₄ compared to the insulating properties of CoO. The XPS results indicate that the formation of CuO and Co-based spinel phases containing both Co²⁺ and Co³⁺ in these catalysts is in line with the XRD results.

Results from the surface-sensitive XPS valence band are in agreement with our TPR results (Figure 1), which represent bulk analysis and suggest that the reducibility of Cu species improved with increasing Co content while that of Co species is decreased with increasing Cu content in the sample. Further, the gradual changes in the Cu 2p BE, I_s/I_m ratio, and fwhm of main and the satellite peaks suggest a significant modification in the bonding nature and distortion of the Cu²⁺ environment upon Co substitution. Although there is an increase in BE of the Cu 2p core level with increasing Co content, the almost same α' value (1851.7 ± 0.1 eV) suggests that Cu species are essentially in the divalent oxidation state. Nonetheless, the Cu–Cu near-neighbor interaction decreases systematically from CuCoC-1 to CuCoC-5. In other words, an exclusive Cu²⁺–O–Cu²⁺ interaction present in CuCoC-1 changes increasingly toward Cu²⁺–

O—Co^{2+/3+}—O—Cu²⁺ and/or Co³⁺—O—Cu²⁺—Co³⁺ type interaction, and this leads to the changes observed in the Cu 2p core level XPS. It is known that, as the distortion of Cu²⁺ environment becomes more significant, the I_s would be enhanced when the coordinating anions are the same.³⁵ Hence, the higher I_s/I_m ratio of CuCoC-4 could be due to a significant distortion in the CuO environment in the present system possibly because of the formation of a Cu-containing Co-spinel such as Cu_xCo_{3-x}O₄ as described earlier on the basis of the XRD data.^{13,35} The high polarizability induced by the presence of Co in these spinel materials would decrease the covalency of the Cu—O bond and improve the reducibility of Cu species, in agreement with the results observed in the TPR. The XRD, TPR, and XPS results therefore strongly suggest the operation of a sort of Cu—Co redox mechanism in these samples and indicate the existence of a synergistic interaction between Cu and Co species.

4.2. Chemical States of Cu and Co in the Reduced Catalysts. As already pointed out, the CuCo-based materials similar to those of the present study have been employed as potential catalysts in a variety of industrially important catalytic processes.^{1–13} In most of these catalytic reactions, including the OSRM reaction, the catalysts are reduced in H₂ around 300 °C prior to the reaction. Hence, Cu and Co in these catalytic systems should be in their reduced states. The in situ XRD demonstrates that the Cu²⁺ is reduced to metallic Cu. However, the Cu metal is reversibly oxidized to Cu₂O when N₂ gas replaces the H₂/Ar gas mixture. This indicates that the presence of even traces of O₂ and/or H₂O in the N₂ gas is sufficient to oxidize a part of metallic Cu to Cu₂O. Additionally, in situ XRD measurements were carried out at atmospheric pressure and not under vacuum. The AES of H₂-reduced catalysts, on the other hand, exhibits peaks corresponding to both Cu⁰ and Cu⁺, indicating the existence of both metallic Cu as well as Cu₂O species on the surface of reduced catalysts although the XRD shows the presence of only metallic Cu. Note, however, that the XRD is a bulk technique while XPS is a surface-sensitive technique. The presence of small Cu₂O (Cu⁺) particles on the surface of the reduced catalysts in the H₂ atmosphere could not have been detected by the in situ XRD under reducing atmosphere.

A comparison of Cu-Auger spectra of reduced samples (Figure 7) clearly indicates that the amount of metallic Cu decreases with increasing Co content in the catalyst. This result hints that the presence of Co favors the stabilization of copper as Cu⁺. The formation of a mixture of Cu⁺ and Cu²⁺ species with Co²⁺ and Co³⁺ species has been noticed by XRD and XPS during calcination, under N₂ atmosphere, of CuCo-binary hydroxycarbonate precursors.^{8,13,35} However, when the same sample was calcined in air, the XRD and XPS indicated the existence of Cu²⁺, Co²⁺, and Co³⁺ species but no Cu⁺ species in the mixed oxides. The above report further supports our hypothesis that the Cu⁺ species can be stabilized in the Co-containing materials if they are treated either in an inert (N₂) or in the reducing atmosphere. Hence, there might be a redox mechanism operating between metallic copper and Co³⁺ species of the spinel. It is likely that, upon H₂-reduction of these catalysts containing a mixture of CuO and Co₃O₄-like spinel at 300 °C, the Cu²⁺ species are reduced first to metallic Cu. This metallic Cu can assist the reduction of Co³⁺ to Co²⁺ during which the metallic Cu is partially oxidized to Cu⁺. In other words, the Co³⁺ species in the spinel partially oxidizes the metallic copper to Cu⁺. The operation of such a redox mechanism could be responsible for the higher activity and oxyanate formation in the methanol and higher alcohol synthesis over the similar CuCo-based mixed oxide catalysts.^{1–5}

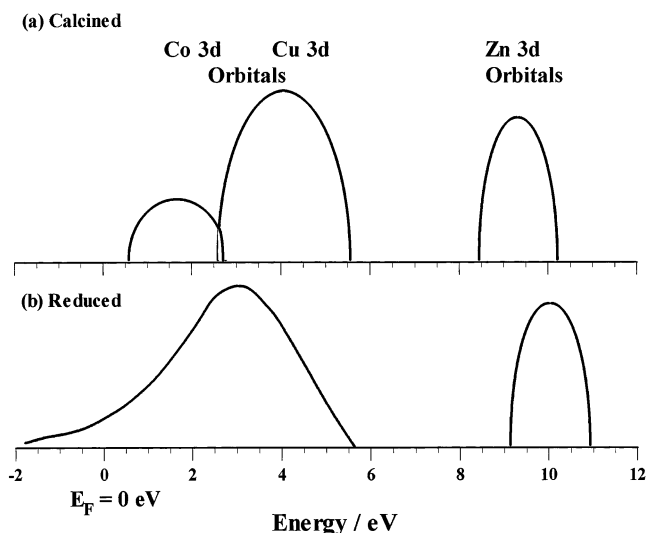


Figure 11. A cartoonist view of energy levels of metal 3d bands in the calcined and reduced CuCoZnAl-mixed oxide catalysts. It is demonstrated that the extent of overlap between Cu 3d and Co 3d bands is weak in calcined materials and strong in the reduced catalysts.

The Co³⁺ species in the Co-based spinel are reduced to Co²⁺, and the resulting material is poorly crystallized. Thus, an amorphous CoO-like species might be present on the surface of these catalysts. This is further supported by an increase in the spin–orbit doublet energy gap from 15 to 15.9 eV from calcined to reduced catalysts (Table 3). Note, however, that the BE and the energy separation of the spin–orbit doublet of reduced catalysts are very close to those of Co(OH)₂ rather than CoO, indicating that the nature of Co on catalysts is similar to that of Co(OH)₂.

4.3. Cu—Co Interaction in the Calcined and Reduced Catalysts. On the basis of core level and VB XPS data of calcined and reduced samples, an energy level diagram has been depicted in Figure 11 to represent the changes qualitatively. It is shown here that the overlap between Cu and Co in the VB region is maximum upon reduction and minimum in the calcined materials. The physicochemical properties of Co-containing catalysts depends on the nature of Co species rather than Cu species since the Co 3d band is the topmost energy level. However, upon reduction, the Cu²⁺ species are reduced to Cu⁰ and Cu⁺ while the Co³⁺ species in the spinel are reduced to Co²⁺. Hence, upon reduction, the Co 3d and Cu 3d VB levels move closer to each other and overlap to a great extent. Thus, the low H₂ production rate of the Co-containing catalyst should be due to the participation of Co species in the hydrogenation activity under reaction conditions. The observed shift in the Zn 3d levels suggests that Zn is involved in the electronic structure and catalytic activity. Further, VB results indicate that the interaction between Cu and Zn species is stronger than that between Co and Zn species.

It is also observed (Figure 9) that metallic copper increases the electron count at E_F , which in turn increases the conductivity of the sample. This might be an important factor responsible for the large H₂ production observed over the Cu-rich catalysts. Notably, the contribution of Cu⁰ to E_F also indicates that the nature of the topmost occupied band has changed from Co 3d in calcined samples to Cu 4s bands on reduced catalysts, and the photoemission near E_F is attributed to Cu 4s bands. Notwithstanding, Co 3d orbital energy is between those of Cu 4s and 3d orbitals. It is well-known that the 4s band in Cu metal is broad and the energy difference between 4s and 3d is small.⁴⁰ In these materials, the central role of Co 3d orbitals is in

overlapping with both the 4s and 3d orbitals of Cu and this point makes the present material integrated electronically. Such an electronic interaction could be responsible for a beneficial catalytic activity reported for the methanol and higher alcohol synthesis^{1–7} and phenol methylation.¹²

Considering the reaction conditions of oxidizing (O₂), reducing (H₂), and partially reducing (H₂O, CH₃OH) agents available at reaction temperatures, it is clear that XPS results of reduced samples apparently resemble those carried out under simulated in situ reaction conditions. This might be a reason for a good correspondence between activity and XPS results, in terms of a large amount of Cu metal observed and H₂ produced from CuCoC-1.

Conclusions

The following major conclusions were drawn from the results obtained in the present study:

1. Thermal decomposition of CuCoZnAl-HT-like precursors produces a mixture of CuO and ZnO phases from the Cu-rich samples. However, the Co-rich samples generate spinel phases similar to Co₃O₄ and/or ZnCo₂O₄ and CuO. Reducibility of CuO is improved with increasing Co content, while the reducibility of Co species is retarded with increasing Cu content.

2. A combined XPS and XAES investigation clearly indicates the existence of Cu²⁺, Co²⁺, and Co³⁺ in the calcined materials. Upon H₂-reduction, the Cu²⁺ is reduced to Cu⁰ and Cu⁺ while Co³⁺ is reduced to Co²⁺. The Cu⁰/Cu⁺ ratio decreases with increasing Co content, indicating the stabilization of Cu⁺ species. The changes observed in the Cu and Co core levels and VB levels and the XAES results corroborate well with XRD and TPR results.

3. The changes observed in the VB region with respect to the Cu/Co ratio of the calcined and reduced catalytic materials offer a clear picture on the overlap of Cu 3d and Co 3d bands and the interaction between Cu and Zn 3d bands. The extent of Cu and Co 3d band overlap is minimum in the calcined samples and it is maximum in the reduced samples. Additionally, Co 3d bands are bridging the energy gap between 4s and 3d bands of Cu in reduced catalysts and this fact highlights the role of Co in the hydrogenation reaction. XPS results unambiguously confirm the existence of a strong interaction between Cu and Co in these materials and thus clearly demonstrate the operation of Cu–Co synergism through overlapping bands.

4. OSRM reaction over these catalysts reveals that the Co-free catalyst offers the highest rate of H₂ production. Introduction of Co decreases the H₂ production rate because the presence of Co favors the CO hydrogenation, thus consuming a part of H₂ produced in the OSRM reaction under the present experimental conditions.

References and Notes

- (1) Cao, R.; Pan, W. X.; Griffin, G. L. *Langmuir* **1988**, *4*, 1108.
- (2) Shefler, G. R.; Jacobson, R. A.; King, T. S. *J. Catal.* **1989**, *116*, 95.
- (3) Baker, J. E.; Burch, R.; Golunski, S. E. *Appl. Catal.* **1989**, *53*, 279.
- (4) Marchi, A. J.; Di Cosino, J. I.; Apesteguia, C. R. *Catal. Today* **1992**, *15*, 383.
- (5) Fornasari, G.; Huysser, A. D.; Mintcher, L.; Trifiro, F.; Vaccari, A. *J. Catal.* **1992**, *135*, 386.
- (6) Figueiredo, R. T.; Lopez Granados, M.; Fierro, J. L. G.; Vidas, L.; Piscina, P. R.; Homs, N. *Appl. Catal. A: Gen.* **1998**, *170*, 145.
- (7) Aquino, A. D.; Cobo, A. J. *Catal. Today* **2001**, *65*, 209.
- (8) Fierro, G.; Jacono, M. L.; Inversi, M.; Dragone, R.; Porta, P. *Top. Catal.* **2000**, *10*, 39.
- (9) Cavani, F.; Trifiro, F.; Vaccari, A. *Catal. Today* **1991**, *11*, 173.
- (10) Zhu, K.; Liu, C.; Ye, X.; Wu, Y. *Appl. Catal. A: Gen.* **1998**, *168*, 365.
- (11) Yumin, L.; Shetian, L.; Kaizhentg, Z.; Xingkai, Y.; Yue, W. *Appl. Catal. A: Gen.* **1998**, *169*, 127.
- (12) Mathew, T.; Shiju, N. R.; Sreekumar, K.; Rao, B. S.; Gopinath, C. S. *J. Catal.* **2002**, *210*, 405.
- (13) Porta, P.; Dragone, R.; Fierro, G.; Inversi, M.; Jacono, M. L.; Moretti, G. *J. Chem. Soc., Faraday Trans.* **1992**, *88*, 311.
- (14) Mathew, T.; Tope, B. B.; Shiju, N. R.; Hegde, S. G.; Rao, B. S.; Gopinath, C. S. *Phys. Chem. Chem. Phys.* **2002**, *4*, 4260.
- (15) Lazar, K.; Mathew, T.; Koppány, Z.; Megyeri, J.; Samuel, V.; Mirajkar, S. P.; Rao, B. S.; Guzzi, L. *Phys. Chem. Chem. Phys.* **2002**, *4*, 3530.
- (16) Cheng, W.-H. *Acc. Chem. Res.* **1999**, *32*, 685.
- (17) Alejo, L.; Lago, R.; Peña, M. A.; Fierro, J. L. G. *Appl. Catal. A: Gen.* **1997**, *162*, 281.
- (18) Breen, J. P.; Ross, J. R. H. *Catal. Today* **1999**, *51*, 521.
- (19) Velu, S.; Suzuki, K.; Osaki, T. *Chem. Commun.* **1999**, 2341.
- (20) Velu, S.; Suzuki, K.; Okazaki, M.; Kapoor, M. P.; Osaki, T.; Ohashi, F. *J. Catal.* **2000**, *194*, 373.
- (21) Velu, S.; Suzuki, K.; Kapoor, M. P.; Ohashi, F.; Osaki, T. *Appl. Catal. A: Gen.* **2001**, *213*, 47.
- (22) Murcia-Mascaros, S.; Navarro, R. M.; Gomez-Sainero, L.; Costantino, U.; Nocchetti, M.; Fierro, J. L. G. *J. Catal.* **2001**, *198*, 338.
- (23) Reitz, T. L.; Lee, P. L.; Czaplewski, K. F.; Lang, J. C.; Popp, K. E.; Kung, H. H. *J. Catal.* **2001**, *199*, 193.
- (24) Velu, S.; Suzuki, K.; Gopinath, C. S.; Hattori, T.; Yoshida, H. *Phys. Chem. Chem. Phys.* **2002**, *4*, 1990.
- (25) Velu, S.; Suzuki, K.; Hashimoto, S.; Satoh, N.; Ohashi, F.; Tomura, S. *J. Mater. Chem.* **2001**, *11*, 2049.
- (26) Velu, S.; Suzuki, K.; Kapoor, M. P.; Tomura, S.; Ohashi, F.; Osaki, T. *Chem. Mater.* **2000**, *12*, 719.
- (27) Severino, F.; Brito, J. L.; Laine, J.; Fierro, J. L. G.; Agudo, A. L. *J. Catal.* **1998**, *177*, 82.
- (28) Moretti, G.; Fierro, G.; Jacono, M. L.; Porta, P. *Surf. Interface Anal.* **1989**, *14*, 325.
- (29) Poulston, S.; Parlett, P. M.; Stone, P.; Bowker, M. *Surf. Interface Anal.* **1996**, *24*, 811.
- (30) Strohmeier, B. R.; Leyden, B. E.; Field, R. S.; Hercules, D. M. *J. Catal.* **1985**, *94*, 514.
- (31) Grohmann, I.; Peplinski, B.; Unger, W. *Surf. Interface Anal.* **1992**, *19*, 591.
- (32) Van der Laan, G.; Westra, C.; Haas, C.; Sawatzky, G. A. *Phys. Rev. B* **1981**, *23*, 4369.
- (33) Zsoldos, Z.; Guzzi, L. *J. Phys. Chem.* **1992**, *96*, 9393.
- (34) Ji, L.; Lin, J.; Zeng, H. C. *J. Phys. Chem. B* **2000**, *104*, 1783.
- (35) Porta, P.; Campa, M. C.; Fierro, G.; Jacono, M. L.; Minelli, G.; Moretti, G.; Stoppa, L. *J. Mater. Chem.* **1993**, *3*, 505.
- (36) Okamoto, Y.; Fukino, K.; Imamaka, T.; Teranishi, S. *J. Phys. Chem.* **1983**, *87*, 3740.
- (37) Yeh, J. J.; Lindau, I. *At. Data Nucl. Data Tables* **1985**, *32*, 1.
- (38) Van Elp, J.; Wieland, J. L.; Esker, H.; Kuiper, P.; Sawatzky, G. A.; de Groot, F. M. F.; Turner, T. S. *Phys. Rev. B* **1991**, *44*, 6090.
- (39) Jimenez, V. M.; Espinos, J. P.; Gonzalez-Eliphe, A. R. *Surf. Interface Anal.* **1998**, *26*, 62.
- (40) Dekker, A. J. *Solid State Physics*; Prentice Hall: London, 1981.